Predicting Post-Disaster Damage Levels and Generating Post-Disaster Imagery from Pre-Disaster Satellite Images Using Pix2Pix

Umut Lagap [1], Saman Ghaffarian [1]

[1] Department of Risk and Disaster Reduction, University College London, Gower Street, London, WC1E 6BT UK
umutlagap@gmail.com, s.ghaffarian@ucl.ac.uk

Keywords: Generative Adversarial Networks (GANs), Pix2Pix, Disaster damage prediction, Remote sensing, Post-disaster imagery.

Abstract

Accurately forecasting disaster impacts before they occur is crucial for effective emergency preparedness and response. This study presents a dual approach utilizing the Pix2Pix conditional Generative Adversarial Network (cGAN) to leverage pre-disaster satellite imagery for enhanced disaster risk management. Firstly, we employ Pix2Pix to predict post-disaster damage levels from pre-disaster satellite images. By training on the xBD dataset, the model learns to generate spatially distributed damage predictions, enabling proactive planning and resource allocation in high-risk areas. Secondly, Pix2Pix is used to generate synthetic post-disaster images from pre-disaster inputs, allowing for scenario visualization without reliance on actual post-disaster imagery. The model's performance is evaluated using accuracy, precision, recall, and F1-score for damage prediction, achieving an accuracy of 79% and an F1-score of 76%. For synthetic image generation, structural similarity index measure (SSIM) and peak signal-to-noise ratio (PSNR) are used, yielding average values of 0.57 and 23.5, respectively. These results indicate the potential of our framework in anticipating disaster damage and generating realistic post-disaster visualizations. The framework's performance depends on the quality and availability of pre-disaster satellite imagery, which may affect prediction reliability. Further evaluation across different disaster types, including earthquakes, and wildfires, is needed to assess robustness and generalizability. This study demonstrates the potential of generative AI-based approaches in enhancing disaster preparedness by providing both damage forecasting and post-disaster image generation. The proposed framework supports decision-makers in emergency response, urban resilience planning, and risk mitigation strategies, contributing to more effective disaster management.

1. Introduction

Disasters continue to threaten communities and cause widespread destruction despite the technological advancements and efforts to build resilience communities (Chaudhary and Piracha, 2021; Rutgersson et al., 2021). Hurricanes are among the most devastating disasters, generating strong winds, heavy rainfall, and storm surges that lead to severe flooding, infrastructure collapse, and widespread displacement (Bender et al., 2010; Van Oldenborgh et al., 2017). This study focuses on hurricane-induced post-disaster damage forecasting and image generation, specifically analyzing the impacts of Hurricanes Florence, Harvey, Michael, and Matthew.

The selected hurricanes represent significant events that caused catastrophic damage across multiple regions including the United States and the Caribbean. Hurricane Florence (2018) produced record-breaking rainfall and severe flooding, particularly in North Carolina, with estimated damage exceeding $25 billion (Paul et al., 2019). Hurricane Harvey (2017) was one of the costliest hurricanes in U.S. history, causing $125 billion in damage, primarily due to extreme flooding in Texas (Omranian et al., 2018). Hurricane Michael (2018) struck the Florida Panhandle as a Category 5 storm, causing $25 billion in damage and widespread structural destruction (Sweeney et al., 2022). Hurricane Matthew (2016) triggered severe flooding across the southeastern U.S., particularly in North and South Carolina, with damages estimated at $7 billion (Ahmed and Memish, 2017).

Accurate disaster planning is crucial to minimizing the adverse effects of disaster-induced damage and enhance post-disaster response and long-term recovery efforts (Alexander, 2015). Following disasters, manual data collection is often inefficient, labor-intensive, and slow, making it unsuitable for large-scale disasters where timely action is critical (Deng and Wang, 2022; Kaur et al., 2023). Remote sensing data provides a more efficient alternative, offering wide-area coverage and insights without the need for on-the-ground surveys (Ghaffarian et al., 2018; Ghaffarian and Kerle, 2019). However, post-disaster remote sensing images are often delayed, unavailable, or expensive, limiting their immediate applicability.

Traditional damage assessment methods rely on post-disaster remote sensing images and manual interpretation, which are time-consuming and require significant human effort (Yu et al., 2018). To address this, automated machine learning models have been developed for post-disaster damage detection (Ghaffarian et al., 2019). For example, Cooner et al. (2016) applied machine learning methods such as Random Forests to earthquake damage following 2010 Haiti earthquake by using high-resolution multispectral and panchromatic imagery and achieved over 77% of accuracy. Rahnemoonfar et al. (2021) evaluated the performance of deep learning (DL) methods, including InceptionV3, ResNet50, and Xception, for post-disaster damage detection by using a high-resolution UAV-based dataset collected following Hurricane Harvey (FloodNet), and achieved over 95% accuracy on the testing data. Using high-resolution satellite images from Maxar, Planet, and other sources, Hacıefendioğlu et al. (2024) evaluated four segmentation models: U-Net (Universal Network), LinkNet (Linking Network), PSPNet (Pyramid Scene Parsing Network), and FPN (Feature Pyramid Network) for detecting collapsed buildings following the 6 February 2023 Türkiye earthquakes (Mw 7.7 and Mw 7.6 in Kahramanmaraş) and FPN achieved the highest accuracy (97.3%) and specificity (99.5%). Moreover, Gupta et al. (2019) developed the xBD dataset, a large-scale dataset containing pre- and post-disaster images of earthquakes, hurricanes, floods, and wildfires, has been widely used in post-disaster damage assessment studies. Ahmadi et al. (2024) proposed BD-SKUNet (Selective-Kernel UNets) for building damage assessment using high-resolution satellite images from the xBD dataset and achieved an F1-score of 75.8%. Despite their efficiency, these methods still depend on the availability of actual post-disaster images, restricting their use in proactive disaster planning.

Generative Adversarial Networks (GANs) has been used in post-disaster damage detection domain to address various challenges. Park et al. (2020) proposed a cycle-consistent generative adversarial network (CycleGAN) based data augmentation method to enhance wildfire detection by addressing data imbalance issue between wildfire and non-wildfire images. The study achieved the highest accuracy of 98.27% and an F1-score of 98.16% in wildfire damage detection by generating synthetic wildfire images from non-fire mountain landscapes using CycleGAN. Shim et al. (2022) proposed a super-resolution and semi-supervised learning approach using GANs for road damage detection. The study utilized Super-Resolution GAN (SRGAN) to enhance image clarity and adversarial learning to improve detection performance with limited labeled data and achieved an average mean Intersection over Union (m-IoU) of 81.54% and an F1-score of 79.23%, outperforming baseline supervised models (m-IoU: 78.81%, F1-score: 75.40%). Tilon et al. (2020) proposed an Anomaly Detecting Generative Adversarial Network (ADGAN) for unsupervised building damage detection, using only pre-disaster images to learn normal building conditions and detect anomalies in post-disaster images. The model was trained on the xBD dataset and a UAV-based earthquake dataset, achieving an F1-score of 0.74 for earthquake damage detection and 0.87 for wildfire damage detection. However, the ability of GANs to predict post-disaster damage levels by only using pre-disaster images remains underexplored.

This study presents an approach leveraging the Pix2Pix conditional Generative Adversarial Network (cGAN) to address critical gaps in post-disaster damage forecasting. By utilizing pre-disaster satellite imagery, this method aims to forecast post-disaster damage levels and generate realistic synthetic post-disaster images before they occur, providing an innovative tool for risk assessment and emergency response planning. Unlike traditional deep learning models that depend on actual post-disaster imagery, this approach facilitates proactive disaster preparedness by forecasting potential damage scenarios before a disaster occurs. This dual-model framework not only enhances quantitative and qualitative damage assessments but also serves as a decision-support tool for emergency responders, urban planners, and policymakers in resource allocation, infrastructure resilience, and disaster mitigation strategies. Through this work, we aim to bridge the gap between predictive analytics and actionable disaster management, contributing to more effective, timely, and informed disaster response efforts.

2. Methods and Materials

2.1 Study Area and Dataset

This study utilizes a subset of xBD dataset specifically focusing on hurricane-induced disasters. The dataset includes pre- and post-disaster satellite images for four major hurricanes: Florence (2018), Harvey (2017), Michael (2018), and Matthew (2016) (Gupta et al., 2019). The satellite images in the xBD dataset were collected from Maxar’s WorldView constellation, providing high-resolution remote sensing data (Figure 1). Each image is a 1024 × 1024 RGB (Reg, Green, and Blue) image, with a spatial resolution ranging from 0.3m to 3m, allowing for detailed analysis of post-disaster damage. The dataset includes paired pre- and post-disaster images, and their post-disaster damage levels, enabling models to learn the transformation between undamaged and damaged structures. Post-disaster damage labels for buildings categorized into four classes in the xBD dataset: no damage, minor damage, major damage, and destroyed.

Table 1: Damage level descriptions in Gupta et al., 2019.

Damage Level	Structure description
No Damage	Undisturbed. No sign of water, structural or shingle damage, or burn marks.
Minor Damage	Building partially burnt, water surrounding structure, roof elements missing, or visible cracks.
Major Damage	Partial wall or roof collapse or surrounded by water/mud.
Destroyed	Scorched, completely collapsed, partially/completely covered with water/mud, or otherwise no longer present.

For this study, we reclassified the original dataset into two damage levels to enhance emergency response prioritization:

- **Undamaged**: Includes buildings labeled as “No Damage” and “Minor Damage” in the original dataset.

- **Damaged**: Includes buildings labeled as “Major Damage” and “Destroyed” in the original dataset.

This binary classification helps distinguish areas that will require prompt emergency response following disasters, allowing decision-makers to efficiently allocate resources for rescue, relief, and recovery efforts.

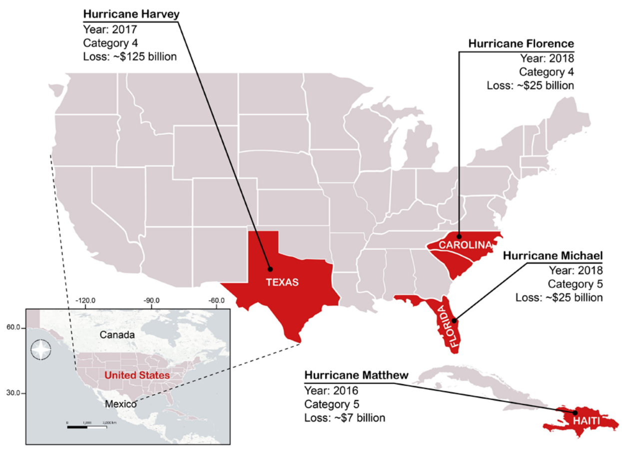

Figure 1: Selected disasters from xBD dataset

2.2 Hurricane-induced post-disaster damage forecast using Pix2Pix

This study introduces a framework utilizing Pix2Pix cGANs to address the limitations of traditional damage detection methods that depend on post-disaster satellite imagery. ModelA predicts post-disaster damage levels using only pre-disaster satellite images, identifying buildings that are likely to be damaged based on learned spatial patterns (Figure 2). ModelB generates synthetic post-disaster satellite images, providing a visual approximation of expected damage to aid in scenario planning and response efforts. By leveraging pre-disaster data, this framework enhances proactive disaster preparedness, enabling more effective risk assessment and resource allocation before an actual disaster occurs.

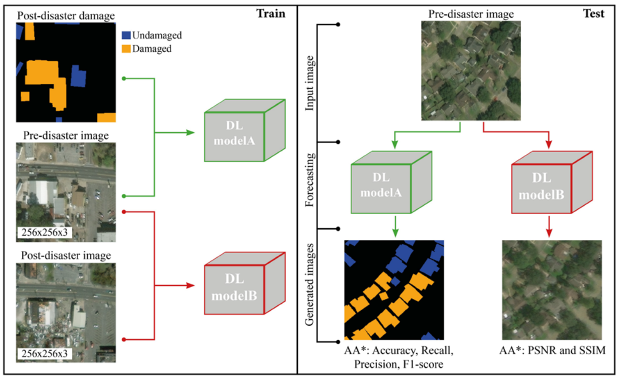

Figure 2: Methodology

Pix2Pix conditions its generation process on an input image, allowing the network to learn structured transformations between pre-disaster and post-disaster images. This is achieved through a conditional adversarial loss, defined as follows:

$$\mathcal{L}_{\text{cGAN}}(G, D) = \mathbb{E}_{(x,y)}[\log D(x, y)] + \mathbb{E}_{x,z}\left[\log\left(1 - D\left(x, G(x, z)\right)\right)\right], \tag{1}$$

$$\mathcal{L}_{L1}(G) = \mathbb{E}_{x,y,z}[\|y - G(x, z)\|_1], \tag{2}$$

where x represents the pre-disaster image, y is the actual post-disaster image from the dataset, $G(x, z)$ denotes the generated post-disaster image, $D(x, y)$ evaluates whether the given pair (x, y) originates from real-world data (Isola et al., 2017).

The first equation represents the conditional adversarial loss, which drives the generator to produce realistic post-disaster images (or damage levels) while allowing the discriminator to distinguish between real and generated images. $L1$ loss minimizes the absolute difference between the generated image $G(x, z)$ and the real post-disaster image or damage level y, ensuring that the generator does not just focus on fooling the discriminator but also closely reconstructs the actual post-disaster scene.

The generator's ultimate goal is to jointly minimize both losses, ensuring that its outputs are both realistic and structurally accurate. $\mathcal{L}_{cGAN}(G, D)$ forces the generator to produce images that fool the discriminator into classifying them as real. $\lambda\mathcal{L}_{L1}(G)$ ensures that the generated images closely match the real post-disaster images on a pixel level. The weighting factor λ controls the trade-off between these two objectives.

$$G^* = \arg\min_G \max_D \mathcal{L}_{cGAN}(G, D) + \lambda\mathcal{L}_{L1}(G), \tag{3}$$

ModelA predicts structural damage at a pixel level rather than classifying entire buildings. Each pixel is assigned a category as undamaged or damaged, enabling fine-grained damage estimation. Since building footprints are known, the mode of all pixels within each building footprint is calculated to determine the final damage level for that structure. This approach ensures that buildings are classified based on the dominant damage category across their pixels, reducing noise and enhancing reliability in damage assessments. Figure 3 shows that the generator follows a U-Net architecture, leveraging skip connections between encoder and decoder layers to retain spatial details. The discriminator uses a PatchGAN structure, classifying small regions (patches) of the damage map rather than evaluating the entire image, leading to enhanced local accuracy. ModelB builds upon the same Pix2Pix framework but generates RGB satellite images instead of damage maps. This model provides a realistic visualization of expected destruction, which is valuable for urban planners, emergency responders, and policymakers.

For computational efficiency, the 1024 x 1024 images were mosaiced into smaller 256 x 256 patches, ensuring that high-resolution details were preserved while making training computationally efficient. The models were optimized using the Adam optimizer (β_1=0.5) with a learning rate of 0.0002, trained for 1000 epochs, and evaluated based on adversarial loss (binary cross-entropy) and L1 loss (mean absolute error). The adversarial loss was assigned a weight of 1, while the L1 loss was given a weight of 100, ensuring a strong emphasis on structural accuracy while maintaining adversarial realism.

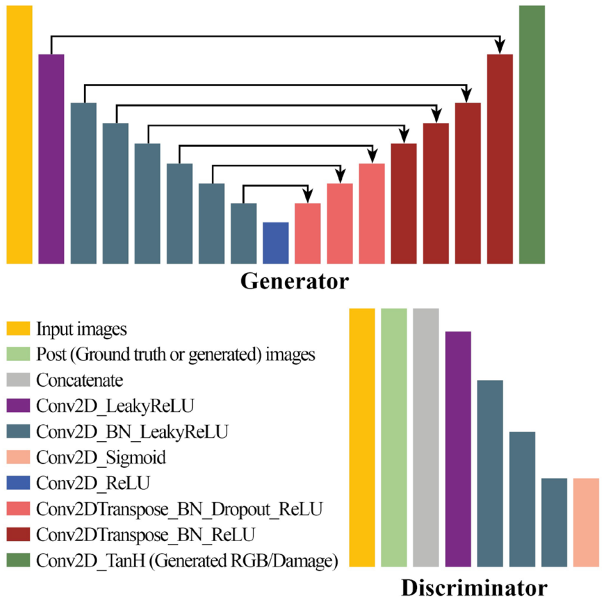

Figure 3: Pix2Pix model architecture.

2.3 Accuracy Assessment

Evaluating the performance of the proposed models requires different assessment metrics based on their respective outputs. Since ModelA focuses on building-level damage classification, it is evaluated using standard classification metrics: Accuracy, Precision, Recall, and F1-score.

$$\text{Accuracy} = \frac{\text{TP} + \text{TN}}{\text{TP} + \text{TN} + \text{FP} + \text{FN}}, \tag{4}$$

$$\text{Precision} = \frac{\text{TP}}{\text{TP} + \text{FP}}, \tag{5}$$

$$\text{Recall} = \frac{\text{TP}}{\text{TP} + \text{FN}}, \tag{6}$$

$$\text{F1 score} = 2 * \frac{\text{Precision} * \text{Recall}}{\text{Precision} + \text{Recall}}, \tag{7}$$

where TP is true positives, TN is true negatives, FP means false positives, and FN represents false negatives.

ModelB generates synthetic post-disaster satellite images, requiring image quality metrics such as Structural Similarity Index Measure (SSIM) and Peak Signal-to-Noise Ratio (PSNR) to assess spatial and pixel-level accuracy. SSIM measures how structurally similar the generated image is to the actual post-disaster image.

$$\mathrm{SSIM}(x, y) = \frac{(2\mu_x\mu_y + C_1)(2\sigma_{xy} + C_2)}{(\mu_x^2 + \mu_y^2 + C_1)(\sigma_x^2 + \sigma_y^2 + C_2)}, \quad (8)$$

where x and y are the generated and real post-disaster images, respectively. μ_x and μ_y represent the mean intensity values of images x and y. σ_x^2 and σ_y^2 are the variance values of the two images. σ_{xy} is the covariance between the two images. Finally, C_1 and C_2 are small constants added to avoid division by zero and stabilize calculations.

PSNR measures the pixel-level accuracy of the generated image by comparing its intensity values to those of the real post-disaster image.

$$\mathrm{PSNR} = 10 \cdot \log_{10}\left(\frac{\mathrm{MAX}^2}{\mathrm{MSE}}\right), \quad (9)$$

where MAX is the maximum possible pixel intensity value. MSE (Mean Squared Error) is calculated as:

$$MSE = \frac{1}{N}\sum_{i=1}^{N}(x_i - y_i)^2, \quad (10)$$

where x_i and y_i are the pixel values of the generated and real images, respectively, and N is the total number of pixels.

3. Results and Discussion

3.1 Building Damage Prediction

The performance of the modelA is evaluated using standard classification metrics: accuracy, recall, and F1-score (Figure 4). The modelA achieved an accuracy of 79% and a precision of 72%, demonstrating a reasonably high capability to forecast post-disaster damage levels based on pre-disaster imagery. The recall score of 80% indicates that the modelA successfully identified most of the actual damaged buildings. The F1-score, which balances precision and recall, stands at 76%, reflecting a well-rounded performance in classifying building damage.

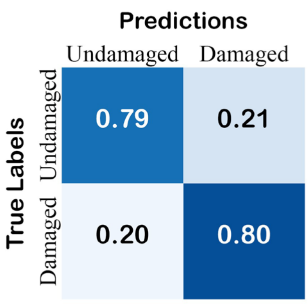

Accuracy	:	0.79
Precision	:	0.72
Recall	:	0.80
F1 score	:	0.76

Figure 4: Confusion matrix

To further assess the performance of ModelA, we present a visual comparison between ground-truth post-disaster damage levels and the model's forecasted damage levels (Figure 5). The top-left image represents the pre-disaster RGB satellite image, while the top-right image displays the corresponding ground-truth damage classification, where blue indicates undamaged buildings and orange denotes damaged buildings. The bottom-left image shows the post-disaster RGB satellite image, which serves as a reference for actual structural changes. The bottom-right image visualizes the model's forecasted damage levels.

The comparison highlights that the model captures large-scale damage patterns effectively, particularly in areas with high building density and clear visibility. However, false classifications are more frequent in zones with mixed land use, possibly due to occlusions or variations in building materials that were not sufficiently learned by the model.

These results highlight the potential of deep learning models in forecasting disaster impacts before they occur, allowing for proactive disaster management strategies. However, some misclassifications still persist, which could be attributed to inherent limitations in the model's ability to distinguish subtle structural vulnerabilities in pre-disaster images.

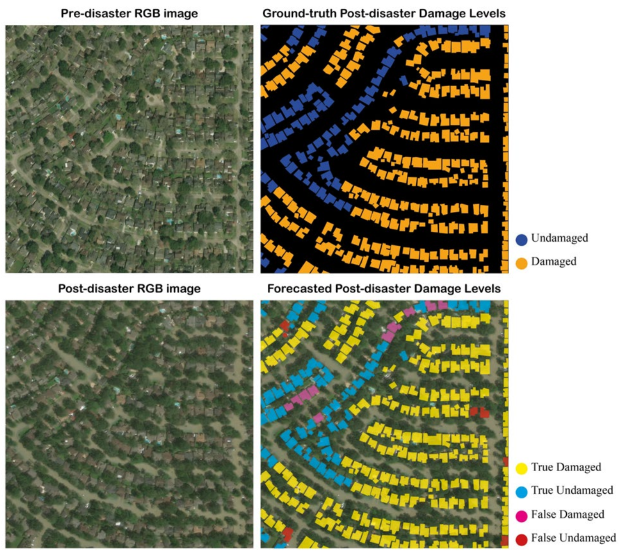

Figure 5: Example comparison of forecasted and ground-truth post-disaster damage levels.

3.2 Post-Disaster Image Generation

ModelB focuses on generating post-disaster imagery from pre-disaster images using Pix2Pix. The performance is evaluated using PSNR and SSIM, where the model achieved an average PSNR of 23.5 and an average SSIM of 0.57. These scores suggest that while the generated images maintain a fair level of structural similarity to actual post-disaster imagery, there are still notable discrepancies.

Figure 6 presents examples of generated post-disaster images from pre-disaster images compared to their corresponding ground-truth post-disaster images. Rows a, b, and c demonstrate successful predictions where the model accurately generated flooding impacts, closely matching the actual post-disaster conditions. However, the model failed to predict flooding in rows d and e, likely due to limitations in learning complex hydrological patterns. It is shown in Rows f and g that the model mistakenly predicted damage as structural destruction rather than flood-related impact. This misclassification suggests that the model has biases towards certain damage types and struggles to differentiate between structural collapse and water-induced damage. Also, the model could not generate successful post-disaster images for highly dense slum areas as shown in Row h. This may be due to challenges in capturing fine-grained structural details and the variability of informal settlements in the dataset.

Figure 6: Pre-disaster images, post-disaster images, generated images.

The results indicate that leveraging pre-disaster imagery for post-disaster image generation provides a valuable tool for early disaster preparedness. By identifying vulnerable structures before a disaster strikes, urban planners and emergency responders can prioritize interventions, allocate resources more efficiently, and mitigate potential losses.

Despite the promising performance, the models exhibit certain limitations. Firstly, false positives (False Damaged) may lead to unnecessary resource allocation, while false negatives (False Undamaged) could result in critical areas being overlooked. Additionally, the model's reliance on visual features alone means that non-visual factors (e.g., construction materials, structural integrity) are not directly accounted for, potentially affecting prediction accuracy. Incorporating supplementary data, such as building metadata or past damage records, could enhance model performance.

4. Conclusions

This study introduced a dual-model framework utilizing Pix2Pix conditional Generative Adversarial Networks (cGANs) for post-disaster damage forecasting and synthetic image generation. By leveraging only pre-disaster satellite imagery, ModelA was designed to predict structural damage levels, while ModelB generated synthetic post-disaster imagery. The results demonstrated that both models provide valuable insights into disaster impact estimation and visualization, offering a potential tool for proactive disaster preparedness and response planning.

The findings of this study have significant implications for disaster risk management. Accurate forecasting of damage levels can help emergency response teams prioritize high-risk areas, allocate resources more efficiently, and improve evacuation planning. Moreover, the ability to generate synthetic post-disaster images allows decision-makers to conduct scenario analyses in regions where actual post-disaster imagery is unavailable. For instance, government agencies can utilize such models to estimate potential damage in hurricane-prone coastal areas, enabling preemptive infrastructure reinforcements. Similarly, humanitarian organizations can identify critical zones requiring immediate assistance, improving relief coordination efforts. Generating synthetic images also eliminates the need for purchasing high-resolution satellite imagery and removes delays associated with satellite tasking and data acquisition, making disaster assessment faster and more cost-effective. Beyond damage prediction, the proposed framework provides a flexible and scalable solution adaptable to different disaster response and recovery needs by replicating the benefits of actual remote sensing imagery.

Despite its potential, this research presents several limitations. The models rely solely on visual features from satellite imagery, without incorporating additional contextual data such as socioeconomic factors, building materials, or structural integrity assessments. This limitation can lead to misclassifications, especially in cases where structural damage is visually subtle. Moreover, the dataset used in training may not generalize well across different disaster types or geographic locations, potentially reducing the model's reliability in unfamiliar regions. Additionally, challenges in predicting flood-related damage and structural damage in highly dense slum areas highlight the need for further refinement in damage differentiation.

Future research should focus on refining the model's ability to differentiate between damage types, particularly distinguishing flood-induced damage from structural destruction. Incorporating post-disaster temporal sequences into the Pix2Pix framework could enhance the model's ability to simulate progressive damage or recovery patterns. Additionally, improving the

https://doi.org/10.5194/isprs-archives-XLVIII-G-2025-861-2025

resolution of generated post-disaster images by modifying the training strategy and loss functions could result in more realistic damage representations. Another potential avenue is to fine-tune the models with region-specific disaster datasets to enhance transferability across different geographic contexts. Leveraging domain adaptation techniques to reduce model bias in underrepresented disaster scenarios could also improve generalizability and robustness in real-world applications.

References

Ahmadi, S. A., Mohammadzadeh, A., Yokoya, N., & Ghorbanian, A. (2024). BD-SKUNet: Selective-Kernel UNets for Building Damage Assessment in High-Resolution Satellite Images. *Remote Sensing, 16*(1), 182. Retrieved from https://www.mdpi.com/2072-4292/16/1/182

Ahmed, Q. A., & Memish, Z. A. (2017). The public health planners' perfect storm: Hurricane Matthew and Zika virus. *Travel Medicine and Infectious Disease, 15*, 63-66. doi:10.1016/j.tmaid.2016.12.004

Alexander, D. E. (2015). Disaster and emergency planning for preparedness, response, and recovery. In: Oxford University Press.

Bender, M. A., Knutson, T. R., Tuleya, R. E., Sirutis, J. J., Vecchi, G. A., Garner, S. T., & Held, I. M. (2010). Modeled impact of anthropogenic warming on the frequency of intense Atlantic hurricanes. *Science, 327*(5964), 454-458. doi:10.1126/science.1180568

Chaudhary, M. T., & Piracha, A. (2021). Natural disasters—origins, impacts, management. *Encyclopedia, 1*(4), 1101-1131.

Cooner, A. J., Shao, Y., & Campbell, J. B. (2016). Detection of Urban Damage Using Remote Sensing and Machine Learning Algorithms: Revisiting the 2010 Haiti Earthquake. *Remote Sensing, 8*(10), 868. Retrieved from https://www.mdpi.com/2072-4292/8/10/868

Deng, L., & Wang, Y. (2022). Post-disaster building damage assessment based on improved U-Net. *Scientific Reports, 12*(1), 15862. doi:10.1038/s41598-022-20114-w

Ghaffarian, S., & Kerle, N. (2019). *Post-disaster recovery assessment using multi-temporal satellite images with a deep learning approach.* Paper presented at the 39th Annual EARSeL Conference & 43rd General Assembly 2019.

Ghaffarian, S., Kerle, N., & Filatova, T. (2018). Remote Sensing-Based Proxies for Urban Disaster Risk Management and Resilience: A Review. *Remote Sensing, 10*(11), 1760. Retrieved from https://www.mdpi.com/2072-4292/10/11/1760

Ghaffarian, S., Kerle, N., Pasolli, E., & Jokar Arsanjani, J. (2019). Post-Disaster Building Database Updating Using Automated Deep Learning: An Integration of Pre-Disaster OpenStreetMap and Multi-Temporal Satellite Data. *Remote Sensing, 11*(20), 2427. Retrieved from https://www.mdpi.com/2072-4292/11/20/2427

Gupta, R., Goodman, B., Patel, N., Hosfelt, R., Sajeev, S., Heim, E., . . . Gaston, M. (2019). *Creating xBD: A dataset for assessing building damage from satellite imagery.* Paper presented at the Proceedings of the IEEE/CVF conference on computer vision and pattern recognition workshops.

Hacıefendioğlu, K., Başağa, H. B., Kahya, V., Özgan, K., & Altunışık, A. C. (2024). Automatic Detection of Collapsed Buildings after the 6 February 2023 Türkiye Earthquakes Using Post-Disaster Satellite Images with Deep Learning-Based Semantic Segmentation Models. *Buildings, 14*(3), 582. Retrieved from https://www.mdpi.com/2075-5309/14/3/582

Isola, P., Zhu, J.-Y., Zhou, T., & Efros, A. A. (2017). *Image-to-image translation with conditional adversarial networks.* Paper presented at the Proceedings of the IEEE conference on computer vision and pattern recognition.

Kaur, N., Lee, C.-C., Mostafavi, A., & Mahdavi-Amiri, A. (2023). Large-scale building damage assessment using a novel hierarchical transformer architecture on satellite images. *Computer-Aided Civil and Infrastructure Engineering, 38*(15), 2072-2091. doi:https://doi.org/10.1111/mice.12981

Omranian, E., Sharif, H. O., & Tavakoly, A. A. (2018). How well can Global Precipitation Measurement (GPM) capture hurricanes? Case study: Hurricane harvey. *Remote Sensing, 10*(7). doi:10.3390/rs10071150

Park, M., Tran, D. Q., Jung, D., & Park, S. (2020). Wildfire-Detection Method Using DenseNet and CycleGAN Data Augmentation-Based Remote Camera Imagery. *Remote Sensing, 12*(22), 3715. Retrieved from https://www.mdpi.com/2072-4292/12/22/3715

Paul, S., Ghebreyesus, D., & Sharif, H. O. (2019). Brief communication: Analysis of the fatalities and socio-economic impacts caused by hurricane florence. *Geosciences (Switzerland), 9*(2). doi:10.3390/geosciences9020058

Rahnemoonfar, M., Chowdhury, T., Sarkar, A., Varshney, D., Yari, M., & Murphy, R. R. (2021). FloodNet: A High Resolution Aerial Imagery Dataset for Post Flood Scene Understanding. *IEEE Access, 9*, 89644-89654. doi:10.1109/ACCESS.2021.3090981

Rutgersson, A., Kjellström, E., Haapala, J., Stendel, M., Danilovich, I., Drews, M., . . . Halsnæs, K. (2021). Natural hazards and extreme events in the Baltic Sea region. *Earth System Dynamics Discussions, 2021*, 1-80.

Shim, S., Kim, J., Lee, S.-W., & Cho, G.-C. (2022). Road damage detection using super-resolution and semi-supervised learning with generative adversarial network. *Automation in Construction, 135*, 104139. doi:https://doi.org/10.1016/j.autcon.2022.104139

Sweeney, K., Wiley, H., & Kousky, C. (2022). The challenge of financial recovery from disasters: the case of florida homeowners after hurricane michael. *Resilience Action Partners and Wharton Risk Management and Decision Processes Center.*

Tilon, S., Nex, F., Kerle, N., & Vosselman, G. (2020). Post-Disaster Building Damage Detection from Earth Observation Imagery Using Unsupervised and Transferable Anomaly Detecting Generative Adversarial Networks. *Remote Sensing, 12*(24), 4193. Retrieved from https://www.mdpi.com/2072-4292/12/24/4193

Van Oldenborgh, G. J., Van Der Wiel, K., Sebastian, A., Singh, R., Arrighi, J., Otto, F., . . . Cullen, H. (2017). Attribution of extreme rainfall from Hurricane Harvey, August 2017.

Environmental research letters, 12(12). doi:10.1088/1748-9326/aa9ef2

Yu, M., Yang, C., & Li, Y. (2018). Big Data in Natural Disaster Management: A Review. *Geosciences, 8*(5), 165. Retrieved from https://www.mdpi.com/2076-3263/8/5/165